Fracture Toughness of Metallic Glasses: Annealing-Induced Embrittlement

Chris H. Rycroft and Eran Bouchbinder

Phys. Rev. Lett. **109**, 194301 — Published 7 November 2012

DOI: 10.1103/PhysRevLett.109.194301

Fracture Toughness of Metallic Glasses: Annealing-induced Embrittlement

Chris H. Rycroft[1,2] and Eran Bouchbinder[3]
[1] *Department of Mathematics, University of California, Berkeley, CA 94720, United States*
[2] *Department of Mathematics, Lawrence Berkeley Laboratory, Berkeley, CA 94720, United States*
[3] *Chemical Physics Department, Weizmann Institute of Science, Rehovot 76100, Israel*

Quantitative understanding of the fracture toughness of metallic glasses, including the associated ductile-to-brittle (embrittlement) transitions, is not yet available. Here we use a simple model of plastic deformation in glasses, coupled to an advanced Eulerian level set formulation for solving complex free boundary problems, to calculate the fracture toughness of metallic glasses as a function of the degree of structural relaxation corresponding to different annealing times near the glass temperature. Our main result indicates the existence of an elasto-plastic crack tip instability for sufficiently relaxed glasses, resulting in a marked drop in the toughness, which we interpret as annealing-induced embrittlement transition similar to experimental observations.

The mechanical properties of glassy materials still pose challenges of great scientific and technological importance. One such fundamental property is the fracture toughness – the ability of a material to resist failure in the presence of a crack [1]. Theoretically predicting the fracture toughness is a particularly pressing problem in the context of metallic glasses. Metallic glasses constitute a promising new class of materials, possessing superior properties, whose usage in structural applications is severely limited by their relatively low fracture toughness [2–8, 11].

Recent observations demonstrated a marked drop in the fracture toughness of metallic glasses as a function of composition and degree of structural relaxation (controlled through annealing near the glass temperature T_g) [6, 9–13]. The drop in the toughness, commonly correlated with Poisson's ratio [11–13], is interpreted as a ductile-to-brittle (embrittlement) transition [9–13], which is not yet well understood.

In this Letter we calculate the fracture toughness of metallic glasses based on the low-temperature Shear-Transformation-Zone (STZ) model, using an advanced Eulerian level set formulation for solving complex free boundary problems. We demonstrate the existence of an elasto-plastic crack tip instability as a function of increasing degree of structural relaxation, which results in a drop in the fracture toughness. We interpret this instability as annealing-induced embrittlement transition similar to the experimental observation.

The STZ model of amorphous plasticity [14–17] has been recently shown to emerge within a systematic formulation of non-equilibrium thermodynamics [18, 19] and to capture a wide range of glassy deformation phenomena [17, 20–24]. Its main advantage in our context is that it offers a way to quantify the degree of structural relaxation and the deformation-driven evolution of structural disorder. Our goal here is to use the model in a way that goes beyond previous analyses; rather than fixing the model parameters to quantitatively describe a given phenomenon, we treat it as a predictive model where its parameters are estimated from independent sources and another phenomenon – crack initiation – is studied.

We focus here on a simple version of the STZ model, retaining only salient physical ingredients. As we are interested in the fracture toughness well below the glass temperature T_g, we neglect all spontaneous, non-driven, relaxation processes and set the plastic rate of deformation $\boldsymbol{D}^{pl}$ to zero for stresses below the shear yield stress s_y, the minimal stress needed to achieve steady state plastic deformation [14]. For $\bar{s} \geq s_y$ we have

$$\boldsymbol{D}^{pl}(\boldsymbol{s}, T, \chi) = \tau_0^{-1} \Lambda(\chi)\, \mathcal{C}(\bar{s}, T)\, [1 - s_y/\bar{s}]\, \boldsymbol{s}/\bar{s}\ , \quad (1)$$

where $\boldsymbol{s} = \boldsymbol{\sigma} - \frac{1}{3}\mathrm{tr}\boldsymbol{\sigma}\, \boldsymbol{1}$ is the deviatoric stress tensor ($\boldsymbol{\sigma}$ is the Cauchy stress) and $\sqrt{2}\,\bar{s} \equiv \sqrt{s_{ij} s_{ij}}$ [16, 17]. $\boldsymbol{D}^{pl}$ is expressed as a product of physically meaningful terms. τ_0^{-1} is a molecular vibration rate. $\Lambda(\chi)$ is the probability to find a structural fluctuation that is particularly susceptible to shear-driven rearrangements – an STZ. It is a function of an effective disorder temperature χ, to be discussed below. $\mathcal{C}(\bar{s}, T)$ quantifies the rate in which STZ's undergo shear transformations and the last terms represent deformation-induced anisotropy ("back stress"), making the whole expression tensorially consistent.

χ characterizes the out-of-equilibrium structural degrees of freedom of a glass [18], generalizing the concept of a fictive temperature [25, 26]. It satisfies an effective heat equation [15, 18]

$$\tau_0 \dot{\chi} = \Gamma(\bar{s}, \chi)\, (\chi_\infty - \chi)\ , \quad (2)$$

where again spontaneous thermally-activated relaxation is neglected. χ_∞ is the steady state value of χ and $\Gamma(\bar{s}, \chi)$ is represents mechanically-generated noise that tends to rejuvenate the glass. This theoretical framework predicts that $\Lambda(\chi)$ in Eq. (1) is determined by a generalized Boltzmann factor, $\Lambda(\chi) = \exp(-e_z/k_B\chi)$, where e_z is the STZ formation energy. It is this description of structural disorder that makes the STZ model most suitable for studying the phenomenon of interest.

We now need to specify explicit forms for $\mathcal{C}(\bar{s}, T)$ and $\Gamma(\bar{s}, \chi)$. The latter was proposed to be proportional to the rate of plastic work $D^{pl}_{ij} s_{ij}$ [17], i.e. $\Gamma(\bar{s}, \chi) =$

$\tau_0 D^{pl}_{ij} s_{ij}/s_y$. $\mathcal{C}(\bar{s},T) \equiv \frac{1}{2}\left[\mathcal{R}(\bar{s},T)+\mathcal{R}(-\bar{s},T)\right]$ is the average of forward and backward STZ transition rates $\mathcal{R}(\pm\bar{s},T) = \exp\left(-\frac{\Delta \mp \Omega\,\epsilon_0\,\bar{s}}{k_B T}\right)$, which we assume to follow a linearly stress-biased thermal activation process. Here Δ is a typical energy activation barrier, Ω is a typical activation volume and ϵ_0 is a typical local strain at the transition [6, 27]. In the presence of the high stresses near a tip of a crack, $\Omega\,\epsilon_0\bar{s}$ may become larger than Δ, in which case we assume the exponential thermal activation form crosses over to a much weaker dependence associated with a linear, non-activated, dissipative mechanism [22]. Hence,

$$\mathcal{C}(\bar{s},T) = \begin{cases} e^{-\Delta/k_B T}\cosh\left[\Omega\,\epsilon_0\,\bar{s}/k_B T\right] & \text{for } \Omega\,\epsilon_0\bar{s} < \Delta \\ \Omega\,\epsilon_0\,\bar{s}/2\Delta & \text{for } \Omega\,\epsilon_0\bar{s} \geq \Delta \end{cases}. \quad (3)$$

As $\Delta \gg k_B T$, the two expressions connect continuously. The slope of the linear relation was chosen so as not to introduce additional parameters. These details do not affect the qualitative nature of the results below.

We adopt an Eulerian formulation and write the rate of deformation tensor as a sum of elastic and plastic contributions, $\boldsymbol{D}^{tot} = \boldsymbol{D}^{el} + \boldsymbol{D}^{pl}$, where $\boldsymbol{D}^{tot} = \frac{1}{2}[\nabla\boldsymbol{v} + (\nabla\boldsymbol{v})^T]$, $\boldsymbol{D}^{el} = \partial_t\boldsymbol{\epsilon} + \boldsymbol{v}\cdot\nabla\boldsymbol{\epsilon} + \boldsymbol{\epsilon}\cdot\boldsymbol{\omega} - \boldsymbol{\omega}\cdot\boldsymbol{\epsilon}$ and $\boldsymbol{\omega} = \frac{1}{2}[\nabla\boldsymbol{v} - (\nabla\boldsymbol{v})^T]$. The strain tensor $\boldsymbol{\epsilon}$ is related to $\boldsymbol{\sigma}$ through Hooke's law $\boldsymbol{\sigma} = K\,\mathrm{tr}\boldsymbol{\epsilon}\boldsymbol{1} + 2\mu\left(\boldsymbol{\epsilon} - \frac{1}{3}\mathrm{tr}\boldsymbol{\epsilon}\boldsymbol{1}\right)$, where K and μ are the bulk and shear moduli, respectively. The velocity field $\boldsymbol{v}(\boldsymbol{r},t)$, where $\boldsymbol{r}$ is the spatial coordinate, evolves through momentum balance $\rho_0\left(\partial_t\boldsymbol{v} + \boldsymbol{v}\cdot\nabla\boldsymbol{v}\right) = \nabla\cdot\boldsymbol{\sigma}$, where ρ_0 is the mass density (assumed constant hereafter).

Consider a blunted straight notch (crack) with root radius ρ (see Fig. 1) under plane-strain conditions. A polar coordinate system (r,θ) is set a distance $\rho/5$ behind the root and $\theta = 0$ is the symmetry axis. We adopt a boundary layer formulation in which the following universal mode I (tensile) crack tip velocity fields are imposed on a scale much larger than ρ [28–32]

$$v_x(r,\theta,t) = \frac{\dot{K}_I(t)}{4\mu}\sqrt{\frac{r}{2\pi}}\left[(5-8\nu)\cos\left(\frac{\theta}{2}\right) - \cos\left(\frac{3\theta}{2}\right)\right],$$
$$v_y(r,\theta,t) = \frac{\dot{K}_I(t)}{4\mu}\sqrt{\frac{r}{2\pi}}\left[(7-8\nu)\sin\left(\frac{\theta}{2}\right) - \sin\left(\frac{3\theta}{2}\right)\right], \quad (4)$$

where $K_I(t)$ is the mode I stress intensity factor and ν is Poisson's ratio [1]. The main advantage of this approach is that the stress intensity factor uniquely couples the inner scales near the tip to the outer scales and hence can be controlled independently without solving the global crack problem [1].

The linear elastic fracture toughness is the critical value of K_I, K_{Ic}, at which the crack initiates and global failure occurs. For multi-component, relatively low cooling rate, bulk metallic glasses this initiation process is less likely to be associated with a fluid meniscus instability [33], but rather with near tip void nucleation [34]. The latter has recently received significant experimental and simulational support [34–38] and is therefore explored here. We interpret the void nucleation process at the continuum level (atomistic aspects might be also relevant [39, 40]) as a local cavitation instability [30] initiating at a structural fluctuation when the hydrostatic tension $\frac{1}{3}\mathrm{tr}\boldsymbol{\sigma}$ exceeds a threshold, which for non-hardening materials is estimated as [41]

$$\sigma_c \simeq 2 s_y \left(1 + \log\left[2\,E/(3\sqrt{3}\,s_y)\right]\right)/\sqrt{3}\,, \quad (5)$$

where E is Young's modulus and $s_y/E \ll 1$.

The model parameters for Vitreloy 1, a widely studied metallic glass used in [12, 13], are estimated from independent sources. We set $\mu = 37$GPa, $\nu = 0.35$, $\rho_0 \simeq 6\mathrm{g/cm}^3$ and $s_y \simeq 0.85$GPa [3, 6]. The basic vibrational timescale is $\tau_0 \simeq 10^{-13}$s. The activation volume of an STZ was estimated to be $\Omega \simeq 1000\mathring{A}^3$ [42] and typically $\epsilon_0 \simeq 0.1$ [6], hence $\Omega\epsilon_0 \simeq 100\mathring{A}^3$. The typical activation barrier is set to $\Delta = 0.7$eV [42]. The STZ formation energy should be somewhat larger than Δ and we set $e_z = 1.8$eV. Finally, χ_∞ is expected to be between $T_g = 623$K and the melting temperature $T_m \simeq 1000$K. Previous works suggest $\chi_\infty \simeq 900$K [22]. We set $T = 400$K, well below T_g.

We set $\dot{K}_I = 10\mathrm{MPa}\sqrt{\mathrm{m}}\,\mathrm{s}^{-1}$ and $\rho = 65\mu$m [12, 13]. A key parameter is the initial value of χ, $\chi(\boldsymbol{r}, t=0) \equiv \chi_0$. In [12, 13], Vitreloy 1 was annealed for different times at T_g and the fracture toughness dropped by an order of magnitude, from $K_{Ic} \simeq 85\mathrm{MPa}\sqrt{\mathrm{m}}$ for the as-cast samples to $K_{Ic} \simeq 8.5\mathrm{MPa}\sqrt{\mathrm{m}}$ for the 12 hours annealed samples. Within the model, we represent the effect of increasing annealing times by decreasing values of the initial effective temperature, and focus on the range $\chi_0 = 600 - 660$K. All other parameters remained fixed.

We solved the equations for $\boldsymbol{\sigma}$, $\boldsymbol{v}$ and χ using the recently proposed Eulerian finite-difference framework, where free boundaries are implicitly tracked by the level set method [43]. A key advantage of this method is its ability to naturally handle topological changes, such as those involved in material failure. The combination of finite-difference and level set methods provides a flexible platform to study complex physical phenomena such as crack initiation and propagation.

The widely separated timescales of elastic and plastic deformations make our equations stiff. In [24], an explicit update procedure, in which the timestep was chosen to be small enough to resolve elastic waves, was employed. It would be prohibitively computationally expensive to access physically relevant timescales using this procedure. We therefore constructed a new numerical scheme in which $\boldsymbol{\sigma}$ and χ are explicitly updated, but $\boldsymbol{v}$ is solved for implicitly using quasi-static force balance $\nabla\cdot\boldsymbol{\sigma} = 0$. Details of the quasi-static scheme and its verification will be given elsewhere. This scheme allows us to use physically realistic loading rates and to dynamically switch to

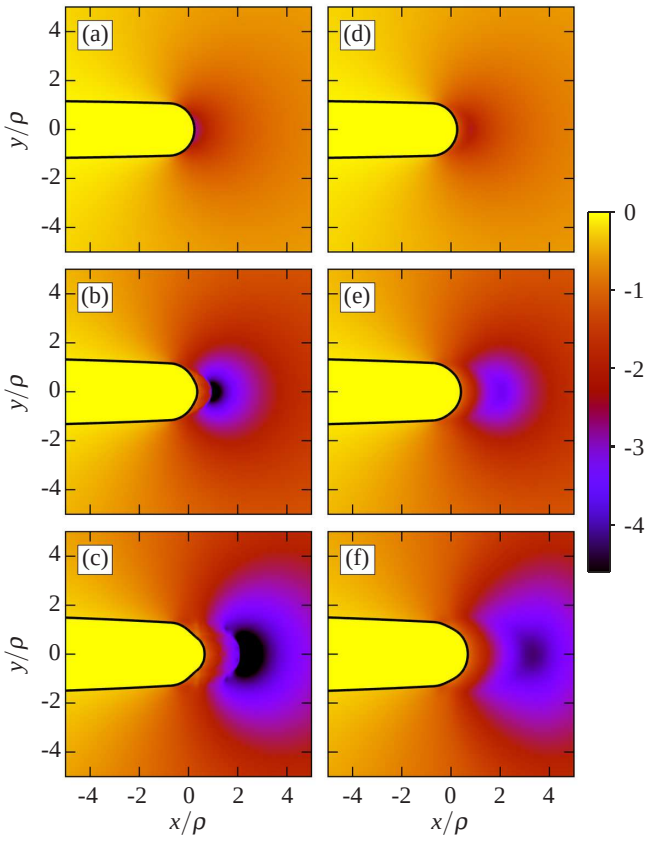

FIG. 1. (Color online) The normalized hydrostatic pressure field p/s_y near a notch at various loading levels $K_I = 20, 40, 60\text{MPa}\sqrt{\text{m}}$ (from top to bottom) for $\chi_0 = 600\text{K}$ (panels a-c) and $\chi_0 = 660\text{K}$ (panels d-f). A movie is available at [51].

the explicit scheme when rapid failure initiates. The calculations presented here employed a $-20 < x/\rho,\, y/\rho < 20$ domain, using a 1025×1025 grid. Increasing grid resolution and/or domain size did not significantly affect the results.

In Fig. 1 we plot a sequence of three snapshots of the hydrostatic pressure field $p(\boldsymbol{r},t) = -\frac{1}{3}\text{tr}\boldsymbol{\sigma}$ for $\chi_0 = 600\text{K}$ (more relaxed) and $\chi_0 = 660\text{K}$ (less relaxed), taken at the same value of K_I. The two sequences seem to exhibit a similar qualitative behavior in which p attains a minimum *ahead* of the notch root at a distance that increases with K_I [29–32]. There are, however, marked quantitative differences: the lower χ_0 exhibits a significantly smaller minimum (accompanied by a sharp spatial variation) and the local notch root radius of curvature decreases, suggesting the onset of a localization process.

To further explore the crack tip dynamics, we plot in Fig. 2 two snapshots of $\chi(\boldsymbol{r},t)$ for each χ_0. Recall that $\chi(\boldsymbol{r},t)$ quantifies structural disorder – the higher χ, the higher the disorder and the easier it is to flow. Both the spatial distribution of χ and the notch geometry are markedly different in the two cases. In the higher χ_0 case, χ is rather smoothly distributed in the near tip region and the notch undergoes continuous blunting – its radius of curvature grows continuously and uniformly with K_I.

The lower χ_0 case is qualitatively different. At small loads, there is little plastic deformation and χ remains nearly constant at its initial value χ_0. As K_I increases, plastic deformation localizes in the root vicinity, resulting in sharply and inhomogeneously distributed χ, featuring small scale filamentary structures. These dynamics are strongly coupled to the notch geometry; the radius of curvature of the notch varies spatially, with a pronounced reduction near the root. It is this localization process – an elasto-plastic crack tip instability – that is responsible for the marked differences in the minima of p in Fig. 1.

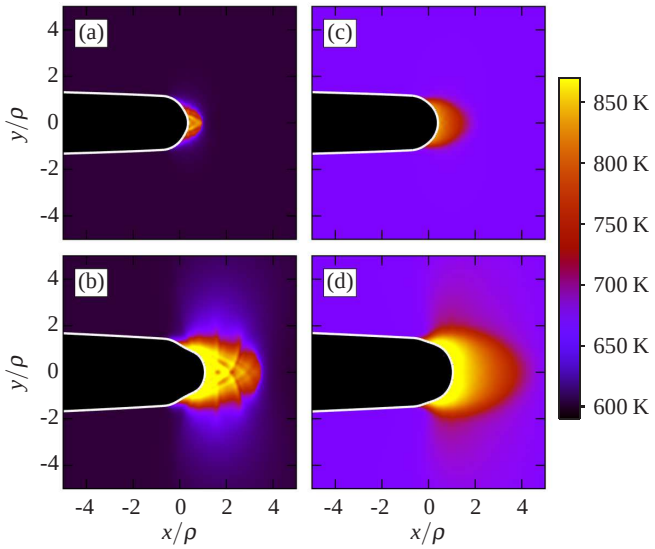

FIG. 2. (Color online) The effective temperature field χ at $K_I = 40\text{MPa}\sqrt{\text{m}}$ (top) and $K_I = 80\text{MPa}\sqrt{\text{m}}$ (bottom) for $\chi_0 = 600\text{K}$ (panels a-b) and $\chi_0 = 660\text{K}$ (panels c-d). A movie is available at [51].

What are the implications of this instability for the fracture toughness? As discussed above, large $|p|$ may induce void nucleation, which might lead to catastrophic failure. Therefore, we focus on the minimum of the pressure $p_{min}(t) \equiv \text{Min}\{p(\boldsymbol{r},t)\}$, shown in Fig. 3a vs. K_I for the two χ_0's. At small K_I both samples respond linear elastically (and hence identically). As K_I increases, local near tip yielding occurs and the curves progressively deviate from the elastic line. Already here quantitative differences are observed: the lower χ_0 sample exhibits less plastic deformation and consequently less stress relaxation and tip blunting, resulting in more negative p_{min}. As K_I further increases, a clear signature of the tip instability discussed above is observed, where p_{min} drops abruptly for the lower χ_0, while the curve for the higher one exhibits smooth and moderate variation with K_I.

A complementary view on the elasto-plastic nature of the instability is obtained by plotting $\chi_{max}(t) \equiv \text{Max}\{\chi(\boldsymbol{r},t)\}$, which quantifies the magnitude of plas-

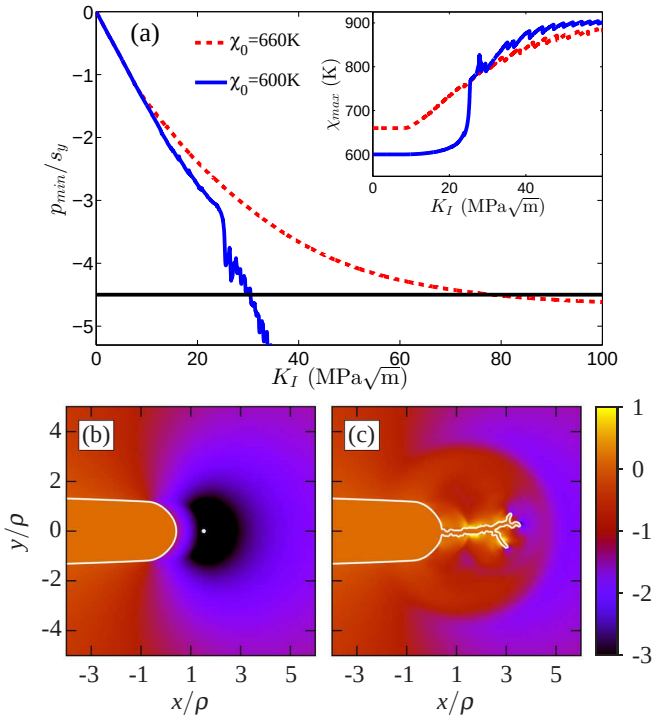

FIG. 3. (Color online) (a) p_{min}/s_y vs. K_I for $\chi_0 = 600$K (solid blue line) and $\chi_0 = 660$K (dashed red line). The horizontal line at $p_{min}/s_y = -4.5$ is the threshold for void nucleation. (inset) χ_{max} vs. K_I (b) A snapshot of the system (p/s_y is plotted) when a void (small white circle) nucleates. (c) The subsequent catastrophic failure. A movie is available at [51].

tic deformation, vs. K_I in the inset of Fig. 3a. For $\chi_0 = 660$K, a linear elastic regime ($\chi_{max} = \chi_0$) is followed by a smooth and moderate increase of χ_{max} toward χ_∞. For $\chi_0 = 600$K the linear elastic regime is followed by an accelerated sharp increase of χ_{max}, which is mirrored in the drop of p_{min} in the main panel. To make things quantitative, we use $E/s_y \simeq 85$ for Vitreloy 1 in Eq. (5) to get $\sigma_c \simeq 5s_y$ [44]. In Fig. 3a, we chose $4.5s_y$ as the threshold (horizontal line) for void nucleation, which suggests a large difference in the fracture toughness, $K_{Ic} \simeq 30\text{MPa}\sqrt{\text{m}}$ for $\chi_0 = 600$K and $K_{Ic} \simeq 80\text{MPa}\sqrt{\text{m}}$ for $\chi_0 = 660$K. Varying σ_c will not change the qualitative nature of this main result, though the flatness of the $\chi_0 = 660$K curve suggests quantitative implications.

Does void nucleation lead to catastrophic failure? i.e. can one interpret K_I at which p_{min} reaches σ_c as the fracture toughness K_{Ic}? To address this issue we take advantage of the model's dynamical nature and the numerical method's flexibility to study the post void nucleation dynamics. A void nucleation is shown in Fig. 3b. The subsequent dynamics, a snapshot of which is shown in panel (c), proceed through a rapid succession of void nucleations, leading to the coalescence of the initial void with the root and to rapid catastrophic failure. This should be contrasted with classical ductile fracture models [45–47], where void growth and coalescence (but not nucleation) limit crack growth rate, leading to slow propagation. The emerging crack pattern in Fig. 3c is reminiscent of some experimental observations [48] (random fluctuations in the void nucleation locations were introduced to avoid artificial grid effects). In light of this catastrophic failure, we interpret the large variation in K_I at which the threshold is met in Fig. 3a for the two different χ_0's as annealing-induced embrittlement transition similar to the experimental observations.

The crack tip instability, which leads to the marked drop in the fracture toughness, has both constitutive and geometric origins. The central physical question here is how efficiently a material can tame the linear elastic stress singularity, associated with the universal crack tip fields of Eqs. (4), by stress relaxation processes [49]. Stress relaxation is mediated both by bulk plastic deformation and by the accompanying geometrical changes in the shape of the notch – the higher the radius of curvature, the lower the stress concentration. As a glass becomes progressively more structurally relaxed (less disordered), these stress relaxation processes become progressively more limited and below some threshold a tip instability sets in.

As mentioned above, the ductile-to-brittle (embrittlement) transition is commonly correlated with Poisson's ratio ν [6, 11, 13]. We suspect that this correlation might not be deep, but rather represents the fact that both the elastic and plastic responses of a glass depend on its state of disorder, quantified here by χ. Hence, while there should exist a configurational equation of state $\nu(\chi)$ [20, 50], its effect on the toughness is expected to be secondary compared to the strong exponential dependence of $\boldsymbol{D}^{pl}$ on $e_z/k_B\chi_0$ through $\Lambda(\chi)$ (the same is expected to apply to the possible χ-dependence of other quantities such as s_y, which was neglected in our calculations). Indeed, for our parameters Λ drops by more than an order of magnitude when χ_0 decreases from 660K to 600K.

The typical fracture toughness values that emerge from our calculations seem to be in the right ballpark, without fine-tuning the model's parameters. We would not, however, take this to imply that our simple model has *quantitative* predictive powers. On the other hand, we do advocate the view that the model can be used to *qualitatively* predict new phenomena, such as the crack tip instability discussed above.

E.B. acknowledges support from the Minerva Foundation with funding from the Federal German Ministry for Education and Research, the Harold Perlman Family Foundation and the William Z. and Eda Bess Novick Young Scientist Fund. C.H.R. was supported by the Director, Office of Science, Computational and Technology Research, U.S. Department of Energy under contract number DE-AC02-05CH11231.

[1] K.B. Broberg, *Cracks and Fracture*, (Academic Press, 1999).
[2] A.L. Greer, Science **267**, 1947 (1995).
[3] W.H. Wang, C. Dong and C.H. Shek, Mater. Sci. Eng. R Rep. **44**, 45 (2004).
[4] M. Telford, Mater. Today **7**, 36 (2004).
[5] M.F. Ashby and A.L. Greer, Scripta Mater. **54**, 321 (2006).
[6] C.A. Schuh, T.C. Hufnagel and U. Ramamurty, Acta Mater. **55** 4067 (2007).
[7] M. Chen, Annu. Rev. Mater. Res. **38**, 445 (2008).
[8] M.M. Trexler and N.N. Thadhani, Prog. Mater. Sci. **55**, 759 (2010).
[9] T.W. Wu and F. Spaepen, Phil. Mag. B **61**, 739 (1990).
[10] P. Murali and U. Ramamurty, Acta Mater. **53**, 1467 (2005).
[11] J. Xu, U. Ramamurty and E. Ma, JOM **62**, 10 (2010).
[12] J.J. Lewandowski, Mater. Trans. JIM **42**, 633 (2001).
[13] J.J. Lewandowski, W.H. Wang and A.L. Greer, Phil. Mag. Lett. **85**, 77 (2005).
[14] M.L. Falk and J.S. Langer, Phys. Rev. E **57**, 7192 (1998).
[15] J.S. Langer, Phys. Rev. E **70**, 041502 (2004).
[16] E. Bouchbinder, J.S. Langer and I. Procaccia, Phys. Rev. E **75**, 036107 (2007).
[17] M.L. Falk and J.S. Langer, Ann. Rev. Cond. Matt. Phys. **2**, 353 (2011).
[18] E. Bouchbinder and J.S. Langer, Phys. Rev. E **80**, 031132 (2009).
[19] E. Bouchbinder and J.S. Langer, Phys. Rev. E **80**, 031133 (2009).
[20] E. Bouchbinder, J.S. Langer and I. Procaccia, Phys. Rev. E **75**, 036108 (2007).
[21] M.L. Manning, J.S. Langer and J.M. Carlson, Phys. Rev. E **76** 056106 (2007).
[22] J.S. Langer, Phys. Rev. E **77**, 021502 (2008).
[23] E. Bouchbinder and J.S. Langer, Phys. Rev. Lett. **106**, 148301 (2011).
[24] C.H. Rycroft and F. Gibou, J. Comp. Phys. **231**, 2155 (2012).
[25] A.Q. Tool, J. Am. Ceram. Soc. **29**, 240 (1946).
[26] L.F. Cugliandolo, J. Phys. A: Math. Theor. **44**, 483001 (2011).
[27] F. Spaepen, Acta Metall. **25**, 407 (1977).
[28] J.R. Rice, J. Appl. Mech. **35**, 379 (1968).
[29] P. Tandaiya, R. Narasimhan and U. Ramamurty, Acta Mater. **55**, 6541 (2007).
[30] D.L. Henann and L. Anand, Acta Mater. **57**, 6057 (2009).
[31] P. Tandaiya, U. Ramamurty and R. Narasimhan, J. Mech. Phys. Solids **57**, 1880 (2009).
[32] R. Narasimhan, H.Y. Subramanya, S.D. Patil, P. Tandaiya and U. Ramamurty, J. Phys. D: Appl. Phys. **42**, 214005 (2009).
[33] A.S. Argon and M. Salama, Mater. Sci. Eng. **23**, 219 (1976).
[34] M.Q. Jiang, Z. Ling, J.X. Meng and L.H. Dai, Phil. Mag. **88**, 407 (2008).
[35] M.L. Falk, Phys. Rev. B, **60**, 7062 (1999).
[36] K.M. Flores and R.H. Dauskardt, Acta Mater, **49**, 2527 (2001).
[37] E. Bouchaud, D. Boivin, J.-L. Pouchou, D. Bonamy, B. Poon and G. Ravichandran, Europhys. Lett. **83**, 66006 (2008).
[38] P. Murali, T.F. Guo, Y.W. Zhang, R. Narasimhan, Y. Li and H.J. Gao, Phys. Rev. Lett. **107**, 215501 (2011).
[39] Q. An, G. Garrett, K. Samwer, Y. Liu, S.V. Zybin, S.N. Luo, M.D. Demetriou, W.L. Johnson and W.A. Goddard, J. Phys. Chem. Lett. **2**, 1320 (2011).
[40] M.L. Falk (private communication).
[41] Y. Huang, J.W. Hutchinson and V. Tvergaard, J. Mech. Phys. Solids **39**, 223 (1991).
[42] H.B. Yu, W.H. Wang and H.Y. Bai, Phys. Rev. B **81**, 220201 (2010).
[43] J.A. Sethian, *Level Set Methods and Fast Marching Methods* (Cambridge, 1996).
[44] E. Bouchbinder, T.S. Lo and I. Procaccia, Phys. Rev. E **77**, 025101 (2008).
[45] F.A. McClintock, J. Appl. Mech. **35**, 363 (1968).
[46] J.R. Rice and D.M. Tracey, J. Mech. Phys. Solids **17**, 201 (1969).
[47] N. Aravas and R.M. McMeeking, J. Mech. Phys. Solids **33**, 25 (1985).
[48] P. Lowhaphandu and J.J. Lewandowski, Scrip. Mater. **38**, 1811 (1998).
[49] M.D. Demetriou, M.E. Laubey, G. Garrett, J.P. Schramm, D.C. Hofmann, W.L. Johnson and R.O. Ritchie, Nat. Mater. **10**, 123 (2011).
[50] J.S. Harmon, M.D. Demetriou, W.L. Johnson and M. Tao, Appl. Phys. Lett. **90**, 131912 (2007).
[51] EPAPS Document No. [*will be added by the editor*]. For more information on EPAPS, see http://www.aip.org/pubservs/epaps.html.